

Triskelion-shaped iridium-helicene NHC complex

Etienne S. Gauthier,^a Nora Hellou,^a Elsa Caytan,^a Samuel Del Fré,^b Vincent Dorcet,^a Nicolas Vanthuyne,^c Ludovic Favereau,^a Monika Srebro-Hooper,^{*b} J. A. Gareth Williams,^d and Jeanne Crassous^{*a}

Received 00th January 20xx,
Accepted 00th January 20xx

DOI: 10.1039/x0xx00000x

Enantiopure tris-helicenic chiral-at-iridium complexes have been prepared, constituting the first examples of organometallic metal-tris-helicenes. They have the *mer*- or *fac*-Ir(C[^]C:)₃ form, where (C[^]C:) is an N-heterocyclic carbene ligand *N*-substituted with a hexahelicene. Their triskelion geometry and stereochemistry have been thoroughly studied and assigned by NMR in combination with quantum-chemical modelling and by comparison with the X-ray structure of analogues. Thanks to their Ir(III)-based multihelicenic architecture, the complexes display strong electronic circular dichroism and optical rotation along with long-lived yellow phosphorescence, involving circularly polarized emission with g_{lum} factors around 10⁻³.

A Introduction

Multihelicenic architectures are currently attracting attention since they are appealing analogues of polycyclic aromatic hydrocarbons (PAHs) and of their heteroatomic versions.^{1a,b,d} These aesthetic, sophisticated, chiral, extended π -conjugated molecules have potential applications in optoelectronics as chiral emitters or semi-conducting materials. However, the construction of such polycyclic systems often requires the use of tedious organic chemistry. While purely organic multiple helicenes have recently appeared in the literature, the precise control of their final structure and related chiroptical properties remains highly challenging.^{1d,2} Conversely, organometallic chemistry enables the development of metal-based helical architectures since a specific metal with an appropriate coordination geometry may give rise to multihelicenic frameworks where the geometry and stereochemistry can be well-controlled.^{1c} For instance, coordination chemistry around an octahedral d⁶ metal ion such as iridium(III) enables three bidentate π -conjugated ligands to be organized in a highly stereomerically controlled fashion, accompanied by the generation of photophysical properties that are appealing for many applications.³

N-Heterocyclic carbenes (NHCs), with their strong σ -donor abilities that enable the formation of stable metal-carbon bonds, constitute an important family of ligands for organometallic and coordination chemistry.⁴ They have been widely applied in homogeneous catalysis,⁵ and more and more

in materials science.^{6,7} Recently, chiral organometallic NHC complexes have emerged as a new class of compounds displaying appealing chiroptical properties including circularly polarized luminescence (CPL),^{7b,8} a feature particularly attractive for applications as chiral emitters for organic light-emitting device (OLED) technology,^{9a} biological imaging,^{9b,c} or chiral sensing.^{9d} As both chemical composition and stereochemical environment may strongly influence the photophysics of a system,⁸ it is of great interest to develop novel chiral molecular materials with highly controlled topologies.

In this research article, we report unprecedented tris-helicenic architectures, formed of one central Ir(III) ion surrounded by three hexahelicene-NHC ligands (see **1a**, **1b**, and **1c** in Figure 1) resulting in unique triskelion (triple-spiral)-shaped complexes. These systems give us the opportunity to investigate the stereoselectivity of the coordination process when using a rather crowded chiral NHC ligand. Complexes bearing all combinations of *fac/mer*, (Δ)/(Λ) and (*M*)/(*P*) configurations can be accessed. They offer scope for a comprehensive study of the photophysical and chiroptical responses of each diastereomerically and enantiomerically pure isomer, *i.e.* electronic circular dichroism (ECD), optical rotation (OR) and CPL spectra. These triskelion molecules have been examined by a combination of NMR, X-ray structures of model analogues, luminescence, (chir)optical spectroscopy, and quantum-chemical calculations. To our knowledge, these are the first molecules successfully organizing three helicenic ligands around a single metal center.^{1c,d}

A Results and discussion

B Synthetic procedures

Our synthetic strategy started with the preparation of methylbenzimidazolium salt **6**, *N*-substituted with a carbo[6]helicenic moiety (Scheme 1a). It followed a well-established route to

^a Univ Rennes, CNRS, ISCR - UMR 6226, F-35000 Rennes, France. Email: jeanne.crassous@univ-rennes1.fr

^b Faculty of Chemistry, Jagiellonian University, Gronostajowa 2, 30-387 Krakow, Poland. Email: srebro@chemia.uj.edu.pl

^c Aix Marseille University, CNRS Centrale Marseille, I5M2, 13284 Marseille, France.

^d Department of Chemistry, Durham University, Durham, DH1 3LE, U.K

† Footnotes relating to the title and/or authors should appear here.

Electronic Supplementary Information (ESI) available: [details of any supplementary information available should be included here]. See DOI: 10.1039/x0xx00000x

benzimidazoles:^{10a} i) a Hartwig-Buchwald coupling to prepare *N*-[6]helicenyl-nitroaniline from 2-bromo-carbo[6]helicene (*rac*)-**2**^{10b} and *ortho*-nitroaniline, ii) a reduction of the nitro group, and iii) cyclization of the obtained *N*-[6]helicene-2-yl-*ortho*-phenylene-diamine to benzimidazole. The Hartwig-Buchwald amination was performed using microwave conditions at 170°C^{10c} and yielded nitro derivative (*rac*)-**3** as bright red crystals in 64% yield after column chromatography. This compound was reduced using tin(II) chloride dihydrate under acidic conditions affording helicenic diamino derivative

(*rac*)-**4**. Owing to its high sensitivity to oxidation, **4** was used directly in the next step without further purification, by heating in triethylorthoformate in the presence of a catalytic amount of TsOH·H₂O, giving (*rac*)-**5** in 68% yield after purification by column chromatography. Note that this compound is a more extended analogue of the previously described [4]helicene-2-*N*-benzimidazole.^{8b}

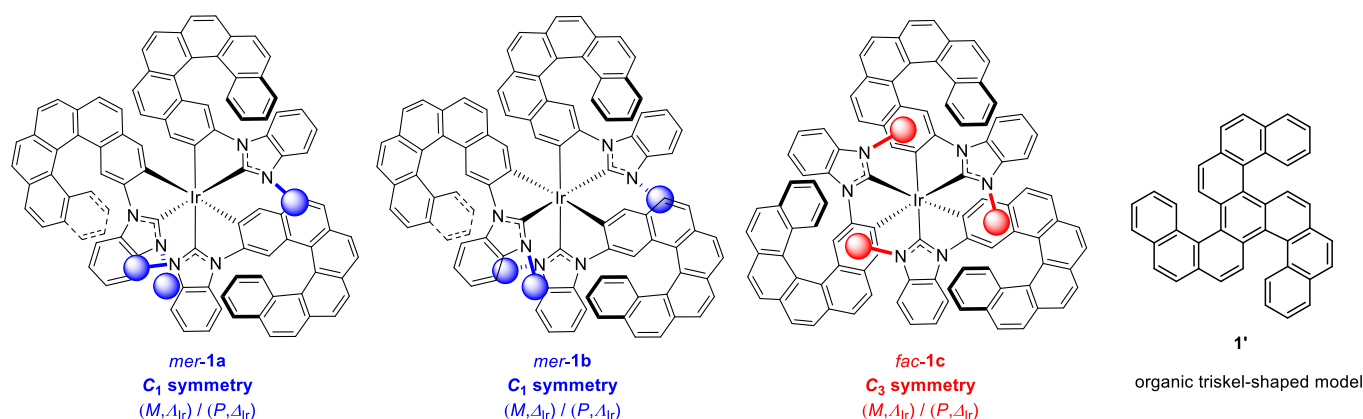
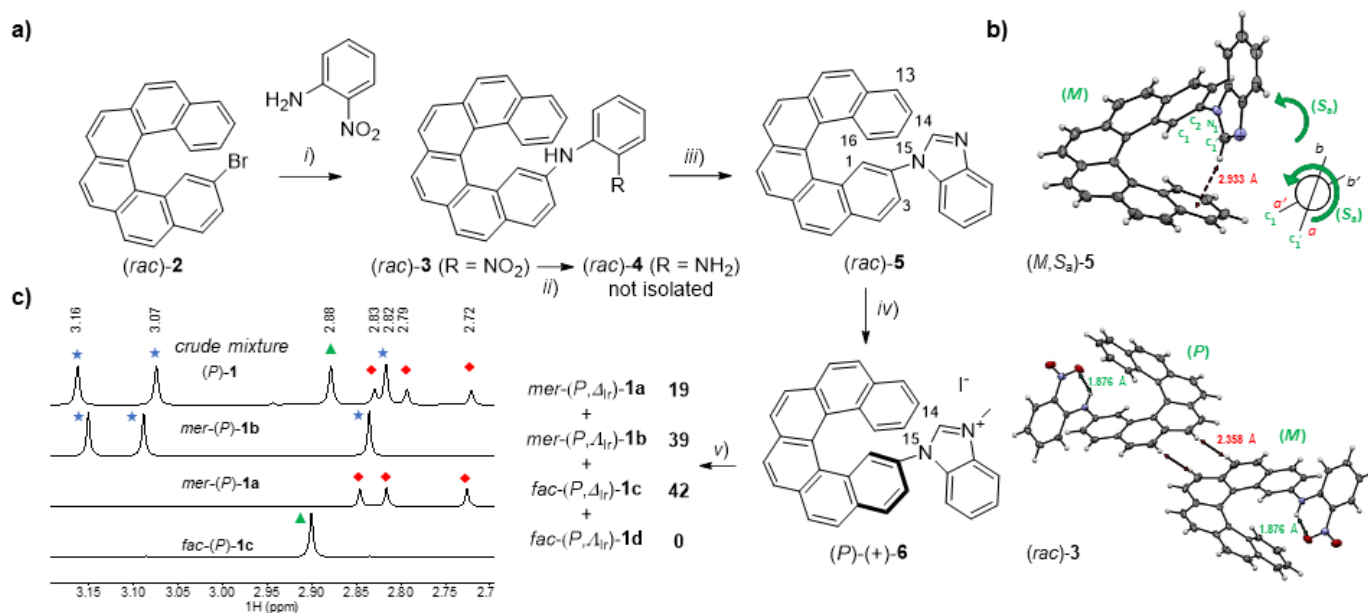


Figure 1. Chemical and stereochemical structure of the prepared chiral *mer* and *fac* tris-helicene-NHC-Ir complexes **1a-c**. Blue and red bawls denote methyl groups. Fully organic triskel-shaped tris-pentahelicenic model **1'**.^{2f}



Scheme 1. a) Synthetic route to helicene-imidazolium salts (*P*)- and (*M*)-**6** and to iridium(III)-tris-helicene-NHC complexes **1a-c**. i) Pd(OAc)₂ / Xantphos (cat.), Cs₂CO₃, toluene, MW, 170°C, 30 min, 64%; ii) SnCl₂·2H₂O, EtOH / HCl (2:1), reflux, overnight; iii) TsOH·H₂O (cat.), (EtO)₃CH, 80°C, overnight, 68% (over 2 steps); iv) chiral HPLC separation, then MeI (excess), MeCN, reflux, overnight; v) Ag₂O, 1,4-dioxane, 60°C, dark, one night, then [Ir(COD)Cl]₂, 120°C, 24 h. b) X-ray crystallographic structures of (*rac*)-**5** (top, only the (*M,S_a*) stereoisomer is shown) and (*rac*)-**3** (bottom). c) ¹H NMR of the Me groups of the (*P*) crude mixture (in CDCl₃) and of the corresponding pure stereoisomers of **1a-c** obtained (in CD₂Cl₂).

All these compounds were fully characterized by NMR analysis and HRMS (see SI). Classical signals of protons on the helicenic unit were observed in CD₂Cl₂, notably H¹⁵ and H¹⁴ (pseudo-triplets at 6.84 and 7.38 ppm, respectively) and H³

(doublet of doublets at 7.43 ppm) for (*rac*)-**5**. Single crystals of (*rac*)-**3** and (*rac*)-**5** suitable for X-ray diffraction were grown by vapor diffusion of *n*-pentane into a solution of the compound in CH₂Cl₂. Both compounds crystallized in the centrosymmetric

space group $P2_1/n$ (Scheme 1b). Their helicities (dihedral angle between terminal rings) of 47.80° and 50.59° , respectively, are typical of hexahelicenes.¹¹ Regarding (*rac*)-**3** (see Scheme 1b bottom), the nitro and the amino groups are nearly coplanar ($N_{\text{nitro}}\text{-C-C-N}_{\text{amine}}$ dihedral angle of 3.16°) and establish intramolecular hydrogen bonding interactions (O-N-O \cdots H-N) that show similar characteristics to those observed for *ortho*-nitroanilines (O \cdots H distance equal to 1.876 \AA , O \cdots H-N angle equal to 136.83°).⁴ The crystal packing is governed by heterochiral interactions, through the aromatic protons located in the central outer part of the helicene (distances of 2.358 \AA); furthermore, an arrangement of homochiral columns stabilized *via* CH- π interactions (distances of 2.770 \AA) appears along the *b* axis (Figure SI.27). In the case of (*rac*)-**5** (Scheme 1b top), interestingly, two stereogenic elements are actually found in the solid state, namely the helicenic unit and the axial chirality around the $N_1\text{-C}_2$ bond ($C_1\text{-N}_1\text{-C}_2\text{-C}_1$ dihedral angle of $\pm 50.53^\circ$) that appears to be associated with an intramolecular CH $\cdots\pi$ interaction established between the $H_{\text{imidazole}}$ and the terminal ring of the helicenic core (2.933 \AA). In the racemic crystal, (*P*) helices are systematically associated with (*R*_a) axial stereochemistry and (*M*) helices with (*S*_a). This confirms that the helical chirality controls the axial chirality through the presence of the intramolecular CH $\cdots\pi$ interaction. Note that such CH $\cdots\pi$ contacts seem to be also present in solution. Indeed, a strongly shielded signal at 6.77 ppm was observed for the $H_{\text{imidazole}}$ in **5** (which shifted to highly deshielded at 9.31 ppm for methyl-imidazolium **6**, *vide infra*). This observation is corroborated by clear NOESY correlation peaks between this proton and the H^1 one in **5** (see ESI). Furthermore, although the rotation around the 2-N bond is probably not fully blocked in solution as suggested by rather broad ^1H signals observed for the whole benzimidazole unit, low temperature NMR (down to 250K) did not yield any splitted signals. Overall, these observations seem to indicate that the (*M,S*_a)/(*P,R*_a) stereoisomers might be stable in solution. Finally, as for (*rac*)-**3**, the supramolecular packing along the *b* axis in the crystal of (*rac*)-**5** is arranged through homochiral columns (Figure SI.28). Hexahelicenic derivative **5** was accessed in enantiopure (*P*)-(+ and (*M*)-(-) forms on 100 mg scale (*ee*'s > 99.5%) after HPLC separation over a chiral stationary phase (Chiralpak IG). Benzimidazolium salts (*P*)-(+ and (*M*)-(-)-**6** were then obtained in > 90% yield by reaction with methyl iodide and used to generate the $[\text{Ir}(\text{C}^{\wedge}\text{C})_3]$ complexes **1**. Following the recently described procedure by Johannes *et al.*,^{12a} the two enantiopure salts (*M*)- and (*P*)-**6** (3 eq.) were engaged in the metalation step by first a reaction with Ag_2O (1 eq.) upon heating (60°C) for one night in the dark, followed by addition of $[\text{Ir}(\text{COD})\text{Cl}]_2$ (0.5 eq.) and further heating (120°C) for 24 h. After a filtration over Celite, the ^1H NMR of the crude mixture of **1** recorded in CDCl_3 showed no deshielded signal around 9-10 ppm confirming the consumption of the benzimidazolium precursor, whilst several new singlets appeared between 2.60 and 3.20 ppm corresponding to the N- CH_3 signals of the desired complexes **1**, formed as a mixture of diastereoisomers **1a**, **1b**, and **1c** (identical singlets were obtained for both (*P*) and (*M*) helicenes, see Scheme 1c, Figures 1, SI.6-SI.9, and NMR analysis presented below).

X-ray analysis of triskelion pentahelicenic-NHC-Ir analogues

All attempts to obtain single crystals of **1a**, **1b** or **1c** failed. However, parallel tests on the synthesis of analogous tris-helicenic $\text{Ir}(\text{C}^{\wedge}\text{C})_3$ complexes, prepared using already reported fused pentahelicenic NHC-based ($\text{C}^{\wedge}\text{C}$:) ligand **7**,^{7a} resulted in a mixture of multiple isomers from which two *fac* complexes could be successfully crystallized and characterized by X-ray crystallography (see *fac*-(*P,M,M*, Δ_{Ir})-**8a** and *fac*-(*P,M,M*, Δ_{Ir})-**8b** in Figure 2). These results provide illustrative insight into the general structural features of the unprecedented triskelion-shaped tris-helicene-NHC-Ir complexes **1**. X-ray crystallography of the pure diastereoisomers **8a** and **8b** ($P2_1/c$ and $P2_1/n$ centrosymmetric space groups, respectively, SI) shows the pseudo-octahedral geometry around the iridium center and the *fac* relationship of the three tolyl rings, whereas the pentahelicene-NHC chelates are oriented in two ways around the Ir(III), defining either the delta (Δ_{Ir}) or lambda (Λ_{Ir}) epimers associated with different helicities, thus yielding *fac*-(*P,M,M*, Δ_{Ir})/(*M,P,P*, Δ_{Ir})-**8a** and *fac*-(*P,M,M*, Δ_{Ir})/(*M,P,P*, Λ_{Ir})-**8b**. The pentahelicene-NHC ligands are bound to one Ir center with classical C-Ir bond-lengths ranging between 2.011 and 2.052 \AA . Furthermore, the tolyl groups are coordinated to the metal *via* their C2' atoms (C2'-Ir between 2.049 and 2.106 \AA) and are almost coplanar with the NHC cycles (dihedral angles between 1.67 and 7.24°). These metric data correspond well with classical values for tris-carbenic cycloiridated $\text{Ir}(\text{C}^{\wedge}\text{C})_3$ complexes,¹² and are very similar to the structural parameters of the computed geometries of the systems **1** (*vide infra*).

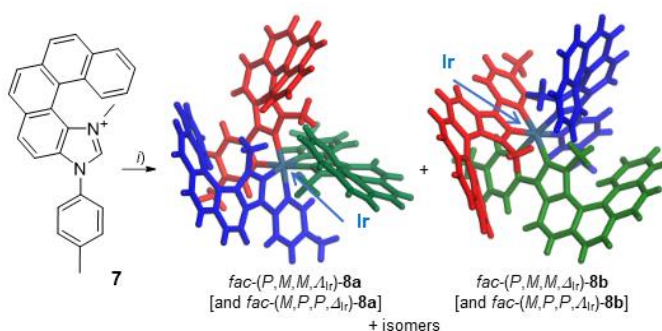


Figure 2. X-ray structures of two *fac* isomers of iridium(III)-tris-[5]helicene-NHC complexes **8a** and **8b** (only one enantiomer is shown) synthesized using ligand **7**. *i*) Ag_2O , $[\text{Ir}(\text{COD})\text{Cl}]_2$, 1,2-dichloroethane, 90°C , dark, 24 h. The red, blue and green colours highlight three different helical branches.

Stereochemical assignment *via* NMR studies

The octahedral complex formed through the cyclometalation of three helicenic NHC ligands with an iridium precursor can be statistically obtained in 32 (2^5) different configurations, due to the helical chirality (*P/M*) of each helicenic ligand (counting for 2^3 possibilities), the chirality-at-iridium ($\Delta_{\text{Ir}}/\Lambda_{\text{Ir}}$) and the two coordination geometries (meridional = *mer*/facial = *fac*). In the present case, the

configuration of the helicene is fixed (either (*P*) or (*M*)), thus reducing the number of statistically possible isomers to pairs of mirror-image compounds:

$mer-(P, \Delta_{Ir})/(M, \Delta_{Ir}) = mer-(P, \Delta_{Ir})/(M, \Delta_{Ir})$ **1a**;

$mer-(P, \Delta_{Ir})/(M, \Delta_{Ir}) = mer-(P, \Delta_{Ir})/(M, \Delta_{Ir})$ **1b**;

$fac-(P, \Delta_{Ir})/(M, \Delta_{Ir}) = fac-(P, \Delta_{Ir})/(M, \Delta_{Ir})$ **1c**;

and $fac-(P, \Delta_{Ir})/(M, \Delta_{Ir}) = fac-(P, \Delta_{Ir})/(M, \Delta_{Ir})$ **1d**

(see Figure 1, Scheme 1c, and discussion below).

From density functional theory (DFT) calculations (TPSS functional coupled with semiempirical dispersion corrections D3, TZVP basis set, continuum solvent model for CH₂Cl₂; see SI for a complete description of the computational protocol applied here), all four isomers were found to be thermodynamically stable and of comparable relative energy values (Table SII.1). However, among these, only 3 pairs of mirror-image isomers were observed in the ¹H NMR spectrum depicted in Scheme 1c, and only one *fac* isomer was found experimentally. Due to the C₃ symmetry of the *fac* isomers, the characteristic protons of the N-CH₃ groups should appear as one singlet integrating to 9 protons, while the spectrum of the *mer* isomers should exhibit 3 different singlets, each integrating to 3 protons, corresponding to the three inequivalent N-CH₃ groups. For each experiment with fixed (*P*) or (*M*) configuration of the helicene ligand, the total number of N-CH₃ ¹H NMR signals in the crude mixture was equal to 7, and not 8. From this, it can be concluded that only three, instead of four, different stereoisomers are obtained: *mer*-**1a,b** and *fac*-**1c** were acquired in respective (19:39:42) and (25:40:35) proportions in the crude (*P*) and (*M*) series (*vide infra*). It is probable that during the reaction performed at high temperature, one *fac* isomer readily transforms to the slightly more stable one.

Each pure stereoisomer could then be successfully obtained from the crude mixture by HPLC separation; overall, they were obtained with *ee*'s higher than 99% and in 2 to 18% yields (see SI). It is noteworthy that for Ir(C[^]C:)₃ complexes hitherto reported, the *mer/fac* ratio of the cyclometalation is close to 4:1,¹² while here it was found to be 58:42 and 65:35 for the crude (*P*) and (*M*) mixture, respectively. The selectivity for the *mer* over the *fac* isomer usually comes from the transient formation of a bridged dimer [Ir(C[^]C:)₂(μ-Cl)]₂ with two ligands in mutually *trans* positions thanks to the *trans* effect.^{12b} In our case, the proximity of two sterically crowded (C[^]C:) hexahelicene units in the *trans* configuration of the μ-chloro dimer is however disfavored, and formation of the *cis* form becomes easier. This helicene-NHC chemistry is thus sufficiently robust to construct three-dimensional architectures with well-defined topologies.

The complete NMR studies (¹H, ¹³C, 2D homonuclear and heteronuclear NMR, performed on 500 MHz or 900 MHz spectrometers) of the optically pure stereoisomers were then conducted in CD₂Cl₂, and the analysis of the resulting NMR signals with reference to the calculated geometries of respective molecular configurations enabled their

stereochemistries to be definitively assigned. As aforementioned, the C₃-symmetric *fac*-(*M*)-**1c** complex displays only one set of ¹H and ¹³C NMR signals for the three equivalent helicene-NHC ligands, with the N-CH₃ methyls protons appearing as a singlet at 2.90 ppm (Scheme 1c) and with the carbenic C atoms giving one signal at 190.6 ppm. Conversely, the ¹H and ¹³C NMR spectra of C₁-symmetric *mer* stereoisomers are richer. For instance, the ¹H NMR spectrum of *mer*-(*M*)-**1b** exhibits three signals at 3.14, 3.08 and 2.83 ppm, readily assigned to the three inequivalent N-CH₃ groups showing in HMBC clear ¹H-¹³C heteronuclear correlations with the three deshielded and distinct carbene atoms (see SI). Additionally, an unambiguous scalar ¹H-¹³C coupling with the proton H⁴ of the ligand **A** (around 6.75 ppm), visible only with the carbene of the ligand **B**, helped to simultaneously assign **B** as the ligand placed *trans* and **C** as the ligand located *cis* to **A** (see Figures 3e and SI.20). Typical signals of the helicene fragment were also identified for *mer*-(*M*)-**1b**, notably H¹⁵ which appears as ddd at 7.33 ppm for ligand **A**, at 6.79 ppm for ligand **B**, and at 6.67 ppm for ligand **C** (see for example Figure 3b).

As the different stereoisomers displayed different NMR spectra, it was of particular interest to know whether – and if yes then how – specific ¹H-¹H homonuclear dipolar correlations between the three helicene ligands might provide information about the stereochemistry at the iridium center. Optimized structures of *mer*-(*M*, Δ_{Ir}), *mer*-(*M*, Δ_{Ir}), *fac*-(*M*, Δ_{Ir}), and *fac*-(*M*, Δ_{Ir}) were thus analyzed in order to search for configurations with selective short distances and NMR correlations, whilst discarding the other stereochemistries that would not correspond to experimental NMR signals. Satisfyingly, the resolution obtained with the different NMR analyses (at 500 MHz and at 900 MHz) was sufficient to find discriminative correlations leading to unambiguous assignment of the stereochemistry of each complex **1a**, **1b**, and **1c**.

As for the C₃-symmetric *fac* isomer, dipolar correlations were found between the N-CH₃ group and the H¹, H¹⁴ and H¹⁵ protons of the helicene unit (Figure 3c). Looking at the optimized *fac* structures and distances presented in Figure 3f and Figure SI.23, it seems unlikely that they originate from protons located on the same ligand, as they are far from each other. Accordingly, these correlations have to stem from through-space interactions between protons of two helicene-NHC ligands located in close proximity. In the *fac*-(*M*, Δ_{Ir}) configuration (Figure SI.23), unlike in *fac*-(*M*, Δ_{Ir}) (Figure 3f), the N-CH₃ group of one ligand appears too far away (> 5 Å) from H¹⁴ and H¹⁵ protons of another ligand to lead to any corresponding dipolar correlations. We can thus conclude that *fac*-(*M*, Δ_{Ir}) (or its enantiomer, *fac*-(*P*, Δ_{Ir})) is the configuration of the complex that fits in the NMR analyses in the case of **1c**, displaying three clear correlation signals between N-CH₃ of one ligand and H¹, H¹⁴ and H¹⁵ of the other ligand, while *fac*-(*M*, Δ_{Ir})/(*P*, Δ_{Ir})-**1d** was not found experimentally.

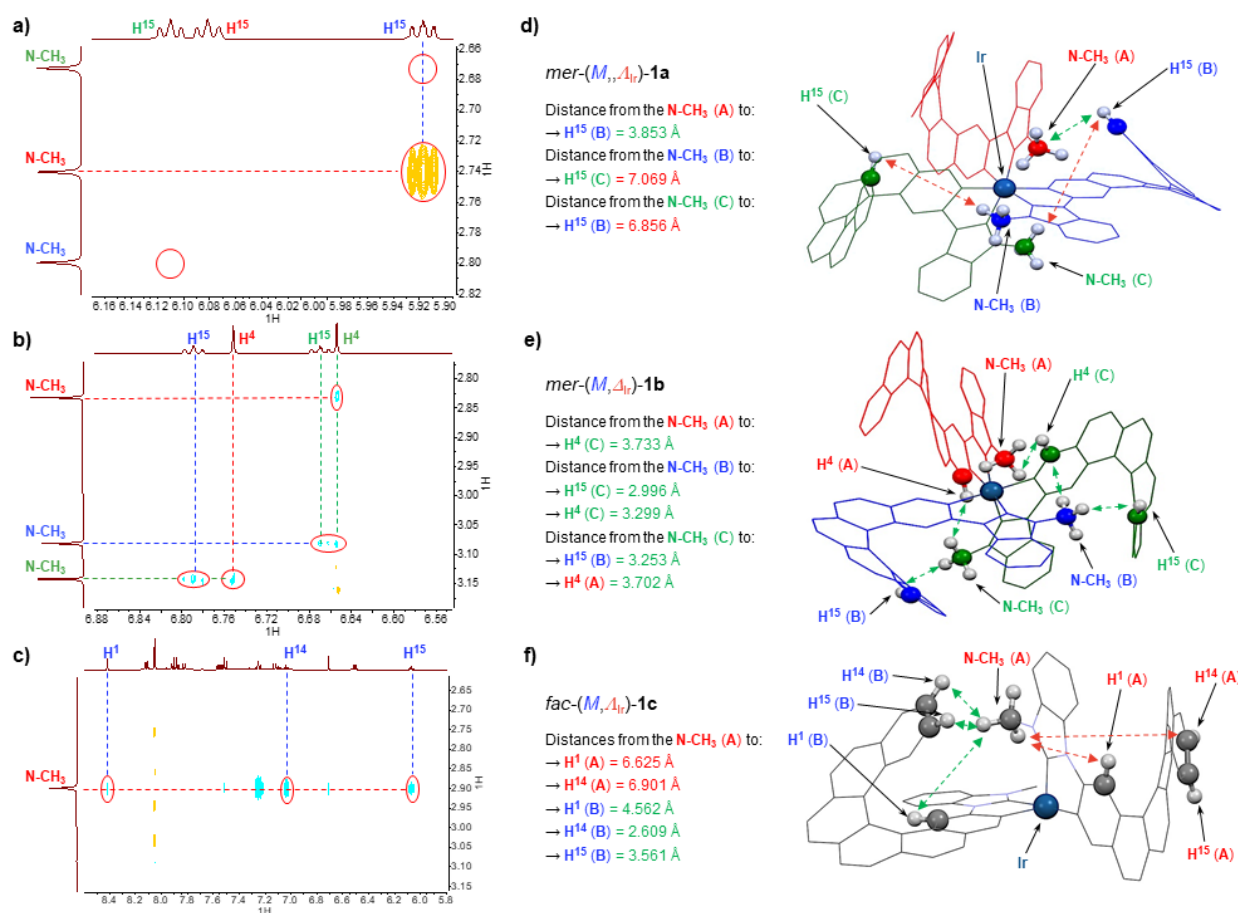


Figure 3. a)-c) ^{1}H - ^{1}H homonuclear correlations observed between the N-CH₃ groups and heliogenic protons (CD_2Cl_2 , 500 or 900 MHz, see SI for precise conditions) in **1a-c**. d)-f) TPSS+D3/TZVP (continuum solvent model for dichloromethane) optimized geometries of $\text{mer}-(M,\Delta_{\text{Ir}})\text{-1a}$, $\text{mer}-(M,\Delta_{\text{Ir}})\text{-1b}$ and $\text{fac}-(M,\Delta_{\text{Ir}})\text{-1c}$ isomers and selected distances (most hydrogen atoms and the third ligand of the *fac* isomer have been omitted for clarity). The three inequivalent hexahelicenic-NHC ligands are denoted **A**, **B** and **C** for clarity. Close distances are highlighted in green, while longer ones are marked in red. See Figure SI.25 for the corresponding 'capped-sticks' representation of each structure, providing a clearer visualization of the 3D arrangement of the ligands.

Regarding the NMR data depicted in Figure 3b for one of the two possible *mer* stereoisomers, the following homonuclear dipolar correlations were noticed: *i*) between the N-CH₃ group of ligand **A** and H⁴ of ligand **C**, *ii*) between the N-CH₃ group of ligand **B** and H¹⁵ and H⁴ of ligand **C**, and *iii*) between the N-CH₃ group of ligand **C** and H¹⁵ of ligand **B** and H⁴ of ligand **A**. Looking at the computed structure of the $\text{mer}-(M,\Delta_{\text{Ir}})$ stereoisomer presented in Figure 3e, we can observe that the respective distances between the denoted N-CH₃ group and the H¹⁵ of the ligands **B** and **C**, as well as the other protons, are below 3.7 Å, which is suitable for spatial correlations. Conversely, considering the $\text{mer}-(M,\Delta_{\text{Ir}})$ configuration depicted in Figure 3d, the distances between the N-CH₃ group of ligands **B** and **C** and H¹⁵ of ligands **C** and **B**, respectively, are longer than 5 Å, which is detrimental to observation of dipolar homonuclear correlations in NMR and corresponds well with the correlations depicted in Figure 3a, *i.e.* only between the N-CH₃ group of ligand **A** and H¹⁵ of ligand **B**. We can thus unambiguously

conclude that the stereochemistry of **1b** is $\text{mer}-(M,\Delta_{\text{Ir}})/(P,\Delta_{\text{Ir}})$, while that of **1a** is $\text{mer}-(M,\Delta_{\text{Ir}})/(P,\Delta_{\text{Ir}})$.

Photophysical properties

The UV-visible absorption spectra of all the stereoisomers **1a-c** were recorded in CH_2Cl_2 solution at room temperature and showed close resemblance to one another (see Figure 4b). For $\text{mer}-(P,\Delta_{\text{Ir}})\text{-1b}$, for example, the band of highest intensity was observed at 275 nm ($\epsilon \sim 90\,000\ \text{M}^{-1}\ \text{cm}^{-1}$), followed by a shoulder centered around 308 nm of nearly half the intensity ($\epsilon \sim 46\,000\ \text{M}^{-1}\ \text{cm}^{-1}$) and a band at 357 nm ($\epsilon \sim 29\,000\ \text{M}^{-1}\ \text{cm}^{-1}$). Weaker, lower-energy signals can also be noticed, centered at 404, 428, and 445 nm ($\epsilon \sim 10\,000$, 4000, and 950 $\text{M}^{-1}\ \text{cm}^{-1}$, respectively).

The general spectral UV-vis envelopes for **1a-c**, along with the close similarities between stereoisomers, are overall

correctly reproduced by TDDFT calculations (PBE0/SV(P) with a continuum solvent model for CH₂Cl₂, see Figure SII.2). The corresponding analysis of molecular orbital (MO) pair contributions to intense excitations confirms the expected π - π^* helicene-centered origin of the intense UV-vis signals but also shows pronounced involvements of the metal d-orbitals and, in the case of higher-energy excitations, the π -orbitals of the NHC units, which constitute metal-to-ligand (ML) and intraligand (IL) charge transfers (CTs), respectively. Importantly, the excitations involve electronic transitions both within a single ligand as well as between ligands, and accordingly feature strong ligand-to-ligand (LL) CT character. In particular, the calculations show that the lowest-energy part of the experimental UV-vis spectra of **1a-c** can be attributed to low-energy excitations which correspond predominantly to transitions between high-lying occupied and low-lying unoccupied MOs (see excitations nos. 1-3 in Figure SII.2, computed at 404-393 nm). Electron density in the high-lying occupied MOs is concentrated mainly at the Ir(III) center and adjacent rings of helicene fragments, while the low-lying unoccupied MOs represent purely helicene-centered π -orbitals either localized at either one of the helicenic NHC ligands (for the C₁-symmetric *mer* stereoisomers **1a** and **1b**) or delocalized over two or all of them (for the C₃-symmetric *fac* structure **1c**); see HOMO-1, HOMO = highest-occupied MO, LUMO = lowest-unoccupied MO, and LUMO+1 presented in Figure 5b for **1a** and **1c**, and SI for a full set of data. Such character of the frontier MOs in **1** clearly reflects extended π -conjugation over the whole molecule and efficient electronic interaction between all three helicenic NHC ligands and the metal center. This may also contribute to the stability of these unprecedented tris-helicenic structures. Accordingly, the low-energy tail in the UV-vis spectra of **1** is due to π - π^* transitions within helicene fragments of ILCT-like nature, due to the fact that the engaged MOs are centered in different parts of the helicenic π -system, accompanied by MLCT and LLCT.

At room temperature in deoxygenated solution, all the complexes **1a-c** exhibit structured yellow luminescence, centered at around 540 nm, with modest quantum yields, Φ , between 1 and 3% (see Table SI.2). The long emission lifetimes under these conditions – between 31 and 81 μ s – are clearly indicative of phosphorescence from the triplet state, as is typical for many tris-cyclometalated Ir(III) complexes. This emission is very strongly quenched upon aeration of the sample, in line with the long excited-state lifetimes. For *fac*-(*P*, Δ)_{Ir}-**1c**, however, additional weaker emission to high energy of the main band is observed that is insensitive to oxygen. The

origin of this emission < 500 nm thus seems likely to be spin-allowed fluorescence from a singlet state. Excitation spectra of *fac*-(*P*, Δ)_{Ir}-**1c** registered at λ_{exc} = 536 and 490 nm (Figure SI.31) both show a good match to the absorption spectra, implying that both emissions do originate from the complex. This dual emission phenomenon was not observed for *mer*-(*P*, Δ)_{Ir}-**1a** or *mer*-(*P*, Δ)_{Ir}-**1b**, which emits only phosphorescence in degassed conditions. (The trace of weak fluorescence around 450 nm for **1a** and, even weaker, for **1b** is almost certainly extraneous and not associated with the complex, based on its high-energy excitation spectrum). Apparently, then, the spin-orbit coupling in the *fac*-(*P*, Δ)_{Ir}-**1c** configuration is not sufficient to make S₁ → T₁ intersystem crossing so fast as to completely eliminate S₁ → S₀ fluorescence. Such dual emission has previously been observed for some platinum(II), iridium(III) and osmium(II) complexes bearing large π -conjugated systems (as is the case here). With increasingly extended conjugation, purer π - π^* character becomes more predominant with an attenuation of the participation of the metal orbitals, and hence a reduction in the efficiency of spin-orbit coupling occurs.¹³ The vibronic progression of around 1300 cm⁻¹ in the phosphorescence spectrum is consistent with largely helicene-centered transitions. The rather low quantum yields can then be readily understood, since a low radiative rate constant is anticipated when the triplet state has little metal character, and non-radiative decay will tend to compete effectively.

The geometry of the complex seems to have an impact on the emission since the phosphorescence lifetime of *mer*-(*P*, Δ)_{Ir}-**1b** is more than twice that of *mer*-(*P*, Δ)_{Ir}-**1a** (81 μ s and 31 μ s, respectively). At 77 K, the emission profiles remain similar, with only a slight blue-shift of around 10 nm relative to room temperature. The suppression of non-radiative pathways under these conditions leads to an increase in the emission lifetimes to around 2 ms for all of the diastereoisomers (Table SI.2). These very long lifetimes are a further reflection of the primarily π - π^* nature of the transitions and of the limited metal contribution. The fact that the phosphorescence lifetimes became independent of the complex's structure at 77 K suggests that the difference between the room temperature lifetimes of *mer*-(*P*, Δ)_{Ir}-**1a** and *mer*-(*P*, Δ)_{Ir}-**1b** arises largely from differing rates of non-radiative decay (Table SI.2). Such a difference might in turn arise from an influence of the complex's geometry on the coupling between electronic and vibrational states or on the extent to which the emissive state interacts with the solvent environment.

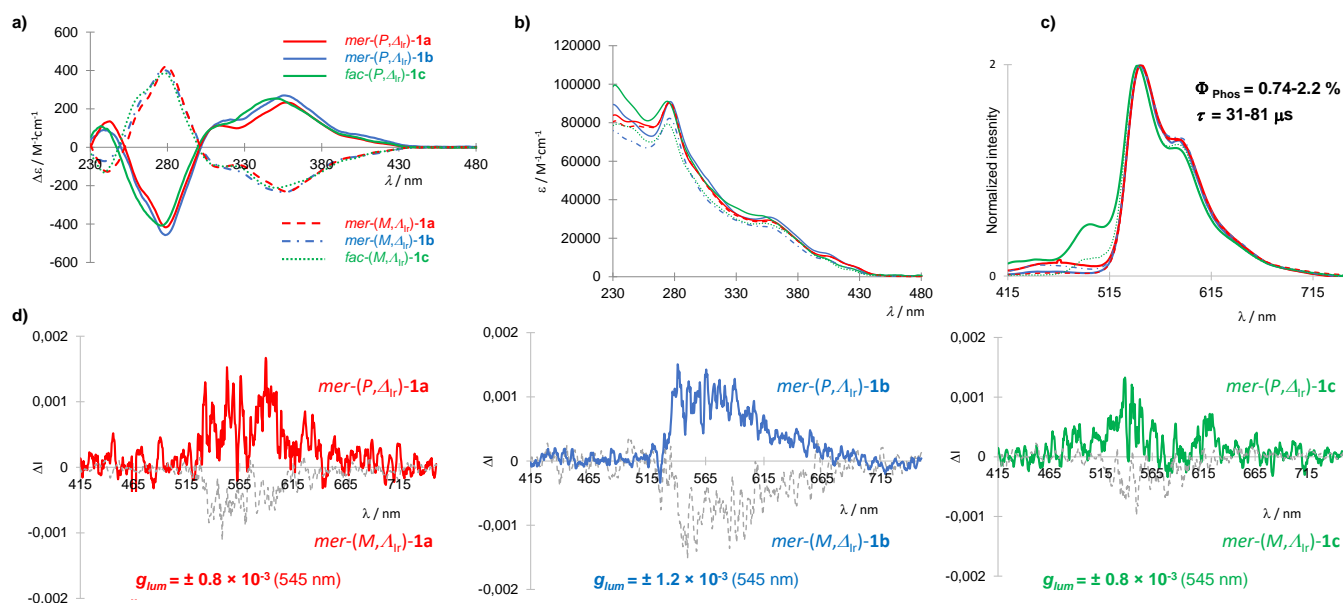


Figure 4. a) Electronic circular dichroism, b) UV-visible absorption, c) luminescence, and d) circularly polarized emission spectra for different stereoisomers of **1a-c** measured in CH_2Cl_2 at 298 K. See also SI.

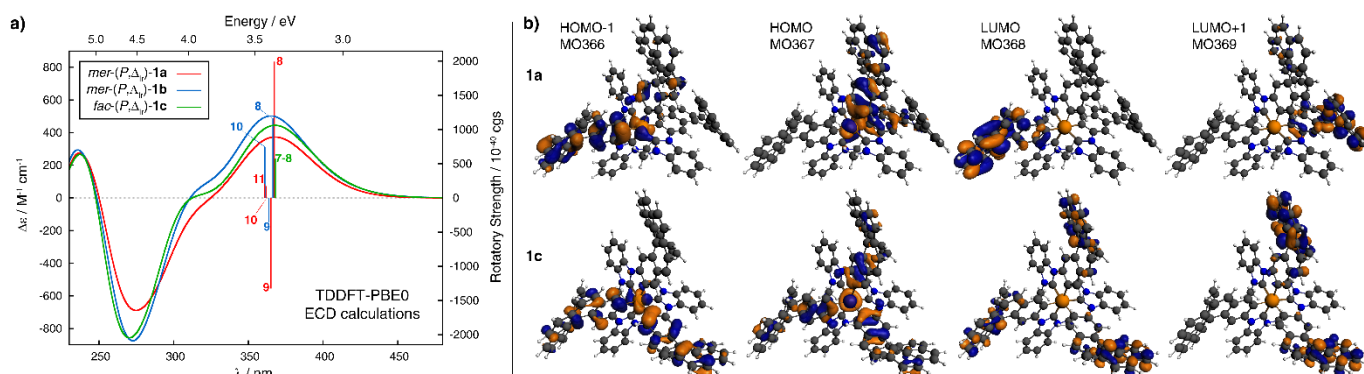


Figure 5. a) Simulated (PBE0/SV(P) with a continuum solvent model for CH_2Cl_2) ECD spectra of **1a-c** with selected excitation energies and rotatory strengths indicated as 'stick' spectra. b) View of frontier MOs for **1a** and **1c** (± 0.03 au). See SI for a full set of computed results.

The TDDFT calculations (PBE0/SV(P) with a continuum solvent model for CH_2Cl_2 , see Table SII.6 and Figure SII.7) of luminescence properties for **1a-c** qualitatively support the experimental assignment of dual fluorescence / phosphorescence emission for **1c**. They also confirm the overall similar phosphorescence energies and predominantly π - π^* helicene-centered character of the emitting T_1 excited state, with a clear MLCT contribution for all three stereoisomers. Interestingly, while for **1c** the triplet state appears to be localized on a single ligand, for both *mer* stereoisomers **1a** and **1b**, it shows some delocalization over two or all of the helicene fragments resulting in LLCT signature in their corresponding $T_1 \rightarrow S_0$ emission transitions. The role of the helicene moiety in influencing the emission properties of its corresponding metallic system has already been observed in recently reported helicenic NHC metal complexes.^{8a,d}

Chiroptical properties

The chiroptical properties (OR, ECD, and CPL) of the Ir(III) complexes **1a-c** were also examined. The high values measured for the molar rotations ($2.5 \times 10^4 - 3.3 \times 10^4$, see SI) are in agreement with data already reported for other multihelicenic organometallic complexes.^{1c,d} Interestingly, all three tris-helicenic systems presented here demonstrate overall similar OR values in spite of their different configurations (chirality-at-iridium and coordination geometry). This might indicate that the contribution of the helical ligand is predominant over the aforementioned configuration-related factors. A synergistic effect of the three helically chiral units linked together is evident, as a 2-fold increase in $[\phi]_D^{25}$ is observed relative to monohelicenes.¹⁰ A similar conclusion can be drawn for the ECD spectra. As shown in Figure 4a for the diastereoisomerically pure complexes, the pairs of enantiomers – *mer*-(M, Δ_{ir})/(P, Δ_{ir})-**1a**, *mer*-(M, Δ_{ir})/(P, Δ_{ir})-**1b**, *fac*-(M, Δ_{ir})/(P, Δ_{ir})-**1c** – display expected mirror-image spectra with strong intensities that for a given configuration of the helicene resemble one another. In line with the similar molar rotation values, this confirms the low

influence of the chirality-at-metal and coordination geometry on the chiroptical properties of these tris-helicenic complexes. For example, *mer*-(*P*, Δ_{Ir})-**1b** exhibits a first positive band at 242 nm ($\Delta\varepsilon = +135 \text{ M}^{-1} \text{ cm}^{-1}$) followed by a strong negative band at 279 nm ($\Delta\varepsilon = -417$). At wavelengths between 300 and 360 nm, the active bands are positive and display slight structure with an increase of intensity from $\Delta\varepsilon = +103 \text{ M}^{-1} \text{ cm}^{-1}$ at 310 nm to $\Delta\varepsilon = +173$ and $+233 \text{ M}^{-1} \text{ cm}^{-1}$ at around 342 nm and 357 nm, respectively. These are then followed by bands of strongly decreased intensity at 402 and 423 nm ($\Delta\varepsilon = +47$ and $+16 \text{ M}^{-1} \text{ cm}^{-1}$, respectively).

The calculations (TDDFT¹⁴ with BHLYP/SV(P) (for OR) and PBE0/SV(P) (for ECD) with a continuum solvent model for CH₂Cl₂) reproduce correctly the large magnitudes and overall similar chiroptical absorption properties of **1a-c** (see Figure 5a and Table SII.2). In particular, the simulated ECD spectra (see Figures 5a and SII.3) agree reasonably well with experiments enabling us to directly disclose an origin of the strong ECD responses and also to comment on structure-property relationships in these complexes. Analysis of intense excitations computed at around 360 nm (see excitations nos. 8-11 (**1a**), 8-10 (**1b**), and 7-8 (**1c**) in Figure 5a) for all three complexes was thus performed. It clearly demonstrated predominant π - π^* helicene-centered character of the main positive band in (*P*)-**1a,b,c** with all the underlying excitations corresponding to CT-like π - π^* transitions within helicene moiety localized at either one of the helicenic NHC ligands, mixed with Ir \rightarrow helicene MLCT and π - π^* helicene \rightarrow helicene transitions engaging different ligands (LLCT). For a complete set of calculated data underlying these assignments, see Tables SII.3-SII.5 and Figures SII.4-SII.6 in SI. Some relevant MOs such as HOMO-1, HOMO and LUMO+1 for **1a** and **1c** are also presented in Figure 5b. Interestingly, in spite of the overall similar electronic character of the dominant excitations computed in this spectral region for all three stereoisomers presented here, the absolute and relative values along with the sign of their corresponding rotatory strength (*R*) appear to be strongly influenced by the chirality-at-iridium and coordination geometry of the system. For example, for *fac*-(*P*, Δ_{Ir})-**1c**, intense excitations around 360 nm demonstrate uniformly positive *R*. On contrast, for the meridional complexes **1a** and **1b**, an excitation with sizable, negative *R* is also present (excitation no. 9 in Figure 5a), and its magnitude is influenced by the chirality at the metal: $\Delta_{\text{Ir}} / A_{\text{Ir}}$ leads to a more negative / less negative value respectively. Consequently, in the case of *mer*-(*P*, Δ_{Ir})-**1a** the ECD intensity of this negative excitation is not completely suppressed by the intensity of surrounding positive excitations, and a noticeable decrease in the main positive ECD band for this stereoisomer compared to other complexes can be seen in Figure 5a, agreeing well with the experimental trend. All this confirms that the strong chiroptical properties in **1a-c** are predominantly a result of synergy in three helical ligands but also clearly indicates that match/mismatch effects of the coordination geometry (*fac* vs. *mer*) and chirality-at-metal (Δ_{Ir} vs. A_{Ir}) are by no means negligible.

Finally, the CPL spectra for all the pairs of pure enantiomeric complexes were recorded. As shown in Figure 4d, they exhibit expected mirror-image CPL activity, with the sign of the CPL

signals dictated by the configuration of the helicene. Indeed, *mer*-(*P*)-**1a,b** and *fac*-(*P*, Δ_{Ir})-**1c** display positive CPL response with g_{lum} (at 545 nm) of ca. $+0.8 \times 10^{-3}$ for *mer*-(*P*, Δ_{Ir})-**1a** and *fac*-(*P*, Δ_{Ir})-**1c** and $+1.2 \times 10^{-3}$ for *mer*-(*P*, Δ_{Ir})-**1b**. Note that precise values are difficult to determine due to the low signal-to-noise ratio in the recorded spectra that results from the rather low quantum yields. Overall the g_{lum} fall within the classical values for chiral organometallic species.

Conclusions

In conclusion, we have prepared and characterized the first tris-helicenic metal complexes. These triskelion-type organometallic systems display *fac/mer*, Δ/Λ and *M/P* stereochemistries; three epimers were obtained, namely, *mer*-(*M*, Δ_{Ir})-**1a**, *mer*-(*M*, Δ_{Ir})-**1b** and *fac*-(*M*, Δ_{Ir})-**1c** (and their corresponding mirror-images). Their full stereochemistries were assigned with the help of homonuclear ¹H NMR correlations and quantum-chemical modelling. These organometallic triskelions are strong absorbers and reveal ECD spectra with magnitude up to $400 \text{ M}^{-1} \text{ cm}^{-1}$. They are also yellow CPL-active phosphors with g_{lum} values around 10^{-3} . The study thus enriches the structural diversity of multiple helicenic systems and opens up new perspectives for developments of novel complexes with controlled stereochemistry and topology. Finally, in the course of the synthesis, a transfer of chirality was observed in the solid state (and potentially in solution) in the *N*-[6]helicene-imidazole derivative, displaying stable helical and axial chirality¹⁶ that will be interesting to exploit in future work.

Author Contributions

E.S.G and N.H performed the synthesis and samples characterizations. LF performed CPL measurements. EC performed and analyzed NMR measurements. VD performed X-ray analyses. N.V. performed HPLC separations. SDF and M.S.-H. performed theoretical calculations. J.A.G.W. performed and analysed emission measurements. J.C. conceived the project, analysed the results and wrote the manuscript with M.S.-H.

Conflicts of interest

“There are no conflicts to declare”.

Acknowledgements

We thank the Centre National de la Recherche Scientifique (CNRS) and the University of Rennes. This work was supported by the Agence Nationale de la Recherche (ANR-16-CE07-0019 “Hel-NHC” grant). M.S.-H. thanks the PL-Grid Infrastructure and the ACC Cyfronet AGH in Krakow, Poland for providing computational resources. The S2wave platform (Univ. Rennes, Building 10A) is acknowledged for the technical support provided during microwave-assisted syntheses. Some of the NMR experiments were performed on the PRISM core Facility

(Biogenouest, UMS Biosit, Université de Rennes 1). Technical and financial support from the IR-RMN-THC FR3050 CNRS for conducting 900 MHz NMR experiments is gratefully acknowledged.

Notes and references

- 1 a) C. Li, Y. Yang, Q. Miao, Recent progress in chemistry of multiple helicenenes. *Chem. Asian J.*, 2018, **13**, 884-894; b) K. Kato, Y. Segawa, K. Itami, Symmetric multiple carbohelicenes. *Synlett*, 2019, **30**, 370-377; c) E. S. Gauthier, R. Rodriguez, J. Crassous, Metal-based multihelicenic architectures. *Angew. Chem. Int. Ed.*, 2020, **59**, 22840-22856; d) T. Mori, Chiroptical properties of symmetric double, triple, and multiple helicenenes. *Chem. Rev.*, 2021, **121**, 2373-2412.
- 2 Selected examples: a) M. Ball, Y. Zhong, Y. Wu, C. Schenck, F. Ng, M. Steigerwald, S. Xiao, C. Nuckolls, Contorted Polycyclic Aromatics. *Acc. Chem. Res.*, 2015, **48**, 267-276; b) Y. Chen, T. Marszalek, T. Fritz, M. Baumgarten, M. Wagner, W. Pisula, L. Chen, K. Müllen, Contorted polycyclic aromatic hydrocarbons with cove regions and zig-zag edges. *Chem. Commun.*, 2017, **53**, 8474-8477; c) T. Hosokawa, Y. Takahashi, T. Matsushima, S. Watanabe, S. Kikkawa, I. Azumaya, A. Tsurusaki, K. Kamikawa, Synthesis, structures, and properties of hexapole helicenenes: assembling six [5]helicene substructures into highly twisted aromatic systems. *J. Am. Chem. Soc.*, 2017, **139**, 18512-18521; d) M. Roy, V. Bereznaia, M. Villa, N. Vanthuyne, M. Giorgi, J.-V. Naubron, S. Poyer, V. Monnier, L. Charles, Y. Carissan, D. Hagebaum-Reignier, J. Rodriguez, M. Gingras, Y. Coquerel, Stereoselective syntheses, structures, and properties of extremely distorted chiral nanographenes embedding hexuple helicenenes. *Angew. Chem. Int. Ed.*, 2020, **59**, 3264-3271; e) K. Kato, Y. Segawa, L. T. Scott, K. Itami, A quintuple [6]helicene with a corannulene core as a C₅-symmetric propeller-shaped π -system. *Angew. Chem. Int. Ed.*, 2018, **57**, 1337-1341; f) H. Tanaka, Y. Kato, M. Fujiki, Y. Inoue, T. Mori, Combined experimental and theoretical study on circular dichroism and circularly polarized luminescence of configurationally robust D₃-symmetric triple pentahelicene. *J. Phys. Chem. A*, 2018, **122**, 7378-7384; g) C. M. Cruz, I. R. Márquez, S. Castro-Fernández, J. M. Cuerva, E. Maçõas, A. G. Campaña, A triskelion-shaped saddle-helix hybrid nanographene. *Angew. Chem. Int. Ed.*, 2019, **58**, 8068-8072.
- 3 a) S. Sprouse, K. A. King, P. J. Spellane, R. J. Watts, Photophysical effects of metal-carbon-sigma-bonds in ortho-metalated complexes of iridium(III) and rhodium(III). *J. Am. Chem. Soc.*, 1984, **106**, 6647-6653; b) K. A. King, P. J. Spellane, R. J. Watts, Excited-state properties of a triply ortho-metalated iridium(III) complex. *J. Am. Chem. Soc.*, 1985, **107**, 1431-1432; c) V. Balzani, A. Credi, F. Scandola, In *Transition Metals in Supramolecular Chemistry*, L. Fabbrizzi, A. Poggi (Eds.), Kluwer: Dordrecht, The Netherlands, 1994; d) V. Balzani, A. Juris, M. Venturi, S. Campagna, S. Serroni, Luminescent and redox-active polynuclear transition metal complexes. *Chem. Rev.*, 1996, **96**, 759-833; e) A. von Zelewsky, *Stereochemistry of Coordination Compounds*, J. & Wiley & Sons, Chichester, 1996; f) A. Amouri, M. Gruselle, *Chirality in Transition Metal Chemistry: Molecules, Supramolecular Assemblies and Materials*, Wiley-VCH, 2009.
- 4 a) D. Bourissou, O. Guerret, F. P. Gabbaï, G. Bertrand, Stable carbenes. *Chem. Rev.*, 2000, **100**, 39-91; b) S. Díez-González (Ed.), *N-Heterocyclic Carbenes: From Laboratory Curiosities to Efficient Synthetic Tools*, RSC: Cambridge, UK; 2011; c) M. N. Hopkinson, C. Richter, M. Schedler, F. Glorius, An overview of N-heterocyclic carbenes. *Nature*, 2014, **510**, 485-496.
- 5 a) S. Díez-González, N. Marion, S. P. Nolan, N-heterocyclic carbenes in late transition metal catalysis. *Chem. Rev.*, 2009, **109**, 3612-3676; b) V. César, S. Bellemin-Laponnaz, L. H. Gade, Chiral N-heterocyclic carbenes as stereodirecting ligands in asymmetric catalysis. *Chem. Soc. Rev.*, 2004, **33**, 619-636; c) F. Wang, L.-J. Liu, W. Wang, S. Li, M. Shi, Chiral NHC-metal-based asymmetric catalysis. *Coord. Chem. Rev.*, 2012, **256**, 804-853; d) D. Zhao, L. Candish, D. Paul, F. Glorius, N-heterocyclic carbenes in asymmetric hydrogenation. *ACS Catal.*, 2016, **6**, 5978-5988.
- 6 a) M. Mercks, M. Albrecht, Beyond catalysis: N-heterocyclic carbene complexes as components for medicinal, luminescent, and functional materials applications. *Chem. Soc. Rev.*, 2010, **39**, 1903-1912; b) R. Visbal, M. C. Gimeno, N-heterocyclic carbene metal complexes: photoluminescence and applications. *Chem. Soc. Rev.*, 2014, **43**, 3551-3574; c) C. A. Smith, M. R. Narouz, P. A. Lummis, I. Singh, A. Nazemi, C.-H. Li, C. M. Crudden, N-heterocyclic carbenes in materials chemistry. *Chem. Rev.*, 2019, **119**, 4986-5056.
- 7 Selected: a) Y. Unger, D. Meyer, T. Strassner, Blue phosphorescent platinum(II) tetracarbene complexes with bis(triazoline-5-ylidene) ligands. *Dalton Trans.*, 2010, **39**, 4295-4301; b) T. Sajoto, P. I. Djurovich, A. Tamayo, M. Yousufuddin, R. Bau, M. E. Thompson, R. J. Holmes, R. S. Forrest, Blue and near-UV phosphorescence from iridium complexes with cyclometalated pyrazolyl or n-heterocyclic carbene ligands. *Inorg. Chem.*, 2005, **44**, 7992-8003; c) S. U. Son, K. H. Park, Y.-S. Lee, B. Y. Kim, C. H. Choi, M. S. Lah, Y. H. Jang, D.-J. Jang, Y. K. Chung, Synthesis of Ru(II) complexes of N-heterocyclic carbenes and their promising photoluminescence properties in water. *Inorg. Chem.*, 2004, **43**, 6896-6898; d) D. Di, A. S. Romanov, L. Yang, J. M. Richter, J. P. H. Rivett, S. Jones, T. H. Thomas, M. A. Jalebi, R. H. Friend, M. Linnolahti, M. Bochmann, D. Credginton, High-performance light-emitting diodes based on carbene-metal-amides. *Science*, 2017, **356**, 159-163; e) R. Hamze, S. Shi, S. C. Kapper, D. S. M. Ravinson, L. Estergreen, M.-C. Jung, A. C. Tadler, R. Haiges, P. I. Djurovich, J. L. Peltier, R. Jazzar, G. Bertrand, S. E. Bradforth, M. E. Thompson, "Quick-silver" from a systematic study of highly luminescent, two-coordinate, d¹⁰ coinage metal complexes. *J. Am. Chem. Soc.*, 2019, **141**, 8616-8626; f) R. Hamze, J. L. Peltier, D. Sylvinson, M. Jung, J. Cardenas, R. Haiges, M. Soleilhavoup, R. Jazzar, P. I. Djurovich, G. Bertrand, M. E. Thompson, Eliminating nonradiative decay in Cu(I) emitters: >99% quantum efficiency and microsecond lifetime. *Science*, 2019, **363**, 601-606; g) M. Deng, N. F. M. Mukthar, N. D. Schley, G. Ung, Yellow circularly polarized luminescence from C₁-symmetrical copper(I) complexes. *Angew. Chem. Int. Ed.*, 2020, **59**, 1228-1231; h) H. Tatsuno, *et al.* Hot branching dynamics in a light-harvesting iron carbene complex revealed by ultrafast X-ray emission spectroscopy. *Angew. Chem. Int. Ed.*, 2020, **59**, 364-372; i) C.-F. Chang, Y.-M. Cheng, Y. Chi, Y.-C. Chiu, C.-C. Lin, G.-H. Lee, P.-T. Chou, C.-C. Chen, C.-H. Chang, C.-C. Wu, Highly efficient blue-emitting iridium(III) carbene complexes and phosphorescent OLEDs. *Angew. Chem. Int. Ed.*, 2008, **47**, 4542-4545; j) P.-H. Lanoë, J. Chan, G. Gontard, F. Monti, N. Armaroli, A. Barbieri, H. Amouri, Deep-red phosphorescent iridium(III) complexes with chromophoric N-heterocyclic carbene ligands: design, photophysical properties, and DFT calculations. *Eur. J. Inorg. Chem.*, 2016, 1631-1634.
- 8 a) N. Hellou, M. Srebro-Hooper, L. Favereau, F. Zinna, E. Caytan, L. Toupet, V. Dorcet, M. Jean, N. Vanthuyne, J. A. G. Williams, L. Di Bari, J. Autschbach, J. Crassous, Enantiopure cycloiridiated complexes bearing a pentahelicenic N-heterocyclic carbene and displaying long-lived circularly-polarized phosphorescence. *Angew. Chem. Int. Ed.*, 2017, **56**, 8236-8239; b) A. Macé, N. Hellou, J. Hammoud, C. Martin, E.

- S. Gauthier, L. Favereau, T. Roisnel, E. Caytan, G. Nasser, N. Vanthuyne, J. A. G. Williams, F. Berrée, B. Carboni, J. Crassous, An enantiopure cyclometallated iridium complex displaying long-lived phosphorescence both in solution and in the solid state. *Helv. Chim. Acta*, 2019, **102**, e1900044; c) N. Hafedh, L. Favereau, E. Caytan, T. Roisnel, M. Jean, N. Vanthuyne, F. Aloui, J. Crassous, Synthesis and chiroptical properties of organometallic complexes of helicenic N-heterocyclic carbenes. *Chirality*, 2019, **31**, 1005-1013; d) E. S. Gauthier, L. Abella, N. Hellou, B. Darquié, E. Caytan, T. Roisnel, N. Vanthuyne, L. Favereau, M. Srebro-Hooper, J. A. G. Williams, J. Autschbach, J. Crassous, Long-lived circularly-polarized phosphorescence in helicene-NHC-rhenium(I) complexes: the influence of helicene, halogen and stereochemistry on emission properties. *Angew. Chem. Int. Ed.*, 2020, **59**, 8394-8400.
- 9 a) D.-W. Zhang, M. Li, C.-F. Chen, Recent advances in circularly polarized electroluminescence based on organic light-emitting diodes. *Chem. Soc. Rev.*, 2020, **49**, 1331-1343; b) J. Zhang, L. Dai, A. M. Webster, W. T. K. Chan, L. E. Mackenzie, R. Pal, S. L. Cobb, G.-L. Law, Unusual magnetic field responsive circularly polarized luminescence probes with highly emissive chiral europium(III) complexes. *Angew. Chem. Int. Ed.*, 2021, **60**, 1004-1010; c) K. Staszak, K. Wieszczycka, V. Marturano, B. Tylkowski, Lanthanides complexes – Chiral sensing of biomolecules. *Coord. Chem. Rev.*, 2019, **397**, 76-90; d) Q. Jin, F. Wang, S. Chen, L. Zhou, H. Jiang, L. Zhang, M. Liu, Circularly polarized luminescence of aluminum complexes for chiral sensing of amino acid and amino alcohol. *Chem. Asian J.*, 2020, **15**, 319-324.
- 10 a) P. Ruiz-Castillo, S. L. Buchwald, Applications of palladium-catalyzed C-N cross-coupling reactions. *Chem. Rev.*, 2016, **116**, 12564-12649; b) D. A. Lightner, D. T. Hefelfinger, T. W. Powers, G. W. Frank, K. N. Trueblood, Hexahelicene. Absolute configuration. *J. Am. Chem. Soc.*, 1972, **94**, 3492-3497; c) M. Jakubec, T. Beránek, P. Jakubík, J. Sýkora, J. Žádný, V. Církva, J. Storch, -Bromo[6]helicene as a key intermediate for [6]helicene functionalization. *J. Org. Chem.*, 2018, **83**, 3607-3616.
- 11 a) C.-F. Chen, Y. Shen, *Helicene Chemistry: From Synthesis to Applications*, Springer Berlin Heidelberg: Berlin, Heidelberg, 2017; b) K. Dhbaibi, L. Favereau, J. Crassous, Enantioenriched helicenes and helicenoids containing main-group elements (B, Si, N, P). *Chem. Rev.*, 2019, **119**, 8846-8953.
- 12 a) J. G. Osiak, T. Setzer, P. G. Jones, C. Lennartz, A. Dreuw, W. Kowalsky, H.-H. Johannes, Twist it! The acid-dependent isomerization of homoleptic carbenic iridium(III) complexes. *Chem. Commun.*, 2017, **53**, 3295-3298; b) C.-H. Chien, S. Fujita, S. Yamoto, T. Hara, T. Yamagata, M. Watanabe, K. Mashima, Stepwise and one-pot syntheses of Ir(III) complexes with imidazolium-based carbene ligands. *Dalton Trans.*, 2008, 916-923; c) J. Lee, H.-F. Chen, T. Batagoda, C. Coburn, P. I. Djurovich, M. E. Thompson, S. R. Forrest, Deep blue phosphorescent organic light-emitting diodes with very high brightness and efficiency. *Nature Mater.*, 2016, **15**, 92-98; d) B. J. Coe, S. J. Glenwright, Trans-effects in octahedral transition metal complexes. *Coord. Chem. Rev.*, 2000, **203**, 5-80; e) S. L. Dabb, N. C. Fletcher, *Mer* and *fac* isomerism in tris chelate dimine metal complexes. *Dalton Trans.*, 2015, **44**, 4406-4422.
- 13 a) D. N. Kozhevnikov, V. N. Kozhevnikov, M. Z. Shafikov, A. M. Prokhorov, D. W. Bruce, J. A. G. Williams, Phosphorescence vs fluorescence in cyclometalated platinum(II) and iridium(III) complexes of (oligo)thienylpyridines. *Inorg. Chem.*, 2011, **50**, 3804-3815; b) P.-T. Chou, Y. Chi, M.-W. Chung, C.-C. Lin, Harvesting luminescence via harnessing the photophysical properties of transition metal complexes. *Coord. Chem. Rev.*, 2011, **255**, 2653-2665; c) Y.-L. Chen, S.-W. Li, Y. Chi, Y.-M. Cheng, S.-C. Pu, Y.-S. Yeh, P.-T. Chou, Switching luminescent properties in osmium-based β -diketonate complexes. *ChemPhysChem*, 2005, **6**, 2012-2017.
- 14 a) M. Srebro-Hooper, J. Autschbach, Calculating natural optical activity of molecules from first principles. *Annu. Rev. Phys. Chem.*, 2017, **68**, 399-420; b) J. Autschbach, Computing chiroptical properties with first-principles theoretical methods: Background and illustrative examples. *Chirality*, 2009, **21**, E116-E152.
- 15 a) B. Doisteau, J.-R. Jiménez, C. Piguet, Beyond chiral organic (p-block) chromophores for circularly polarized luminescence: the success of d-block and f-block chiral complexes. *Front. Chem.*, 2020, **8**, 555; b) L. Arrico, L. Di Bari, F. Zinna, Quantifying the overall efficiency of circularly polarized emitters. *Chem. Eur. J.*, 2021, **27**, 2920-2934.
- 16 A. Macé, K. Hamrouni, E. S. Gauthier, M. Jean, N. Vanthuyne, L. Frédéric, G. Pieters, E. Caytan, T. Roisnel, F. Aloui, M. Srebro-Hooper, B. Carboni, F. Berrée, J. Crassous, *Chem. Eur. J.*, 2021, 10.1002/chem.202100356.